

Fracture Behavior of Functionally Graded Concrete Materials for Rigid Pavements

Jeffery Roesler, Glaucio Paulino, Cristian Gaedicke, Amanda Bordelon,
and Kyoungsoo Park

Currently, in concrete pavements, a single concrete mixture design and structural surface layer are selected to resist mechanical loading without an attempt to affect concrete pavement shrinkage, ride quality, or noise attenuation adversely. An alternative approach is to design sub-layers within the concrete pavement surface that have specific functions and thus to achieve higher performance at a lower cost. The objective of this research was to address the structural benefits of functionally graded concrete materials (FGCMs) for rigid pavements by testing and modeling the fracture behavior of different combinations of layered plain concrete materials and concrete materials reinforced with synthetic fibers. The three-point bending-beam test was used to obtain the softening behavior and fracture parameters of each FGCM. The peak loads and initial fracture energy between the plain, fiber-reinforced, and FGCMs were similar; this signified similar crack initiation. The total fracture energy clearly indicated the improvements in fracture behavior of FGCM relative to full-depth plain concrete. The fracture behavior of FGCM depended on the position of the fiber-reinforced layer relative to the starter notch. The fracture parameters of both the fiber-reinforced and plain concrete were embedded into a finite element-based cohesive zone model. The model successfully captured the experimental behavior of the FGCMs and now can be implemented to predict the fracture behavior of proposed FGCM configurations and structures such as rigid pavements. This integrated approach (testing and modeling) is promising and demonstrates the viability of FGCM for designing layered concrete pavement systems.

Rigid pavement systems are constructed at airports, in high-volume traffic corridors (such as Interstates, highways, and arterials), ports, local streets, and parking lots. The concrete material and rigid pavement structure must be designed to be multifunctional to resist mechanical loadings, resist stresses from thermal and moisture gradients, survive early-age and long-term volumetric changes, attenuate noise, and provide a skid- and wear-resistant and drainable surface layer. Currently, a single monolithic concrete mixture design and structural surface layer are selected in an attempt to optimize the aforementioned objectives by balancing the trade-offs between strength, volumetric stability, and desired surface characteristics. This standard method results in greater slab depths and may not meet all the performance criteria desired for the design.

Department of Civil Engineering, University of Illinois at Urbana-Champaign, 205 North Mathews Avenue, MC-250, Urbana, IL 61801. Corresponding author: J. Roesler, jroesler@uiuc.edu.

Transportation Research Record: Journal of the Transportation Research Board, No. 2037, Transportation Research Board of the National Academies, Washington, D.C., 2007, pp. 40–49.
DOI: 10.3141/2037-04

The research, design, and manufacturing of functionally graded materials (FGMs) have been extensively applied to high-performance materials such as graded metals and composite metals–ceramics for high-technology applications (1–3). The concept of FGMs consists of producing steady transitions in material microstructure and composition to meet the functional requirements of an engineered component and thus to enhance the overall performance of the system (3, 4). An innovative approach that can maximize the performance while minimizing the cost of the concrete pavement is to use layers with different properties at specified depths. By having continuous layers in the concrete pavement, the performance criteria of each layer can be maximized by including them only in the necessary location with the appropriate thickness.

There is an increasing performance demand placed on the materials used to construct, repair, and maintain the pavement infrastructure. However, the availability of high-quality construction materials is diminishing, with the result that lower-quality construction and recycled materials are used. To make use of such materials, a multi-functional and functionally layered (or graded) concrete pavement structure could be constructed to address the multiobjective performance requirements. For example, discrete fibers could be volumetrically graded through the slab depth to improve the fatigue- and fracture-resistant properties in the tensile-loading region of the slab. A different fiber type and volume and larger-size coarse aggregate could be used in the middle or near the surface of the slab to improve the cyclic shear resistance of the concrete joints. Finally, the upper surface layer could contain concrete materials that are both shrinkage and skid resistant. Potentially, this functionally graded concrete pavement system could outperform the existing homogeneous concrete material layer in terms of fatigue, strength, shrinkage, durability, and life cycle costs.

Functionally graded concrete materials (FGCMs) would be constructed in multiple layers (5) by incrementally varying the material properties. The FGCM systems could be practically constructed by modifying existing paving equipment to allow for extrusion of multilayered concrete through a continuous feeding and auguring arrangement or in a precast operation. With this method, the construction of the individual layers is completed when the concrete is still plastic; thus, no discrete interfaces exist in the system.

Building layered pavements is not a new concept in the construction industry. Layered-concrete paving has been used in Europe (6), was constructed in Michigan (7), and has been implemented in other areas of the United States (8). In the majority of these applications, the surface concrete mixture was designed for friction and noise, while a standard concrete paving mixture was used in the lower region of the slab. The primary objectives of the previous multilayered concrete pavement systems were reduced life cycle costs and improved riding surface. Limited research was conducted to test and analyze these layered

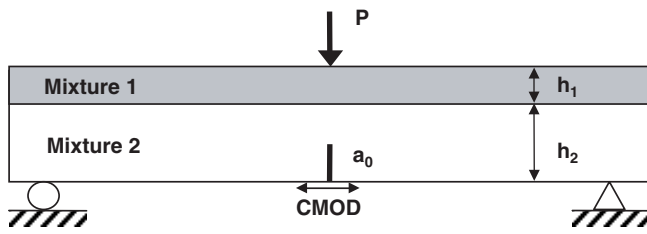


FIGURE 1 TPB test setup for functionally layered concrete specimens.

concrete pavement systems for their mechanical properties. Research on flexural strength and casting delay times have been studied for layered fiber-reinforced concrete beams (9). In addition, research on the interfacial characteristics and fatigue performance of bonded fiber-reinforced overlay systems has been studied (10).

RESEARCH OBJECTIVES AND SCOPE

The objective of this research was to explore the structural benefits of FGCM for rigid pavements by testing and simulating the fracture behavior for different combinations of layered plain and fiber-reinforced concrete (FRC) materials. A numerical model based on the finite element method that used cohesive elements with specific constitutive relations for plain and fiber-reinforced concrete was developed and its results were compared with the experiments. By achieving these objectives, this research demonstrated the viability of functionally graded systems and proposed key concepts required for modeling and designing multilayered concrete pavement systems.

EXPERIMENTAL PROGRAM

Testing Program

The testing program consisted of four specimen configurations to analyze the effect of using different combinations of concrete mixtures [plain portland cement concrete (PCC) and FRC] on the top or bottom layer of the specimen. Three-point bending-beam (TPB) specimens were used, as shown in Figure 1, to characterize the fracture behavior of the individual and functionally layered concrete materials. The concrete fracture parameters, derived from the TPB test, were based on the two-parameter fracture model (TPFM) (11–13) and the Hillerborg work on fracture method (14).

Table 1 lists the material combinations used for the TPB testing program. The materials used for each layer are defined in accordance with the mixture identifications (Mixture ID) in Table 2. Two-beam configurations have the same concrete material in the top and bottom layer so as to characterize the fracture parameters of the individual materials. Three-beam replicates were made for each material configuration.

TABLE 1 Material Combinations Used in Experimental Testing Program

Configuration ID	PCC-PCC	PCC-FRC	FRC-PCC	FRC-FRC
Top layer (h_1)	PCC	PCC	FRC	FRC
Bottom layer (h_2)	PCC	FRC	PCC	FRC

TABLE 2 Concrete Mixture Proportions and 7-Day Strength Properties of Layer Materials Used in Experimental Testing Program

Mixture ID	Plain Concrete		Fiber-Reinforced Concrete	
	PCC	FRC	PCC	FRC
Material	kg/m ³	lb/yd ³	kg/m ³	lb/yd ³
Water	183	308	183	308
Type I cement	360	607	360	607
Coarse aggregate	976	1,645	976	1,645
Fine aggregate	807	1,360	807	1,360
Synthetic fibers	—	—	7.2	12.1
Properties	MPa	Psi	MPa	Psi
Compressive strength (f_c)	33.1	4,799	31.4	4,551
Split tensile strength (f_t)	3.44	499	4.22	612

Mix Design and Properties

Two concrete mixtures were cast for this comparative study of FGCM: PCC and FRC. The mixture proportions are presented in Table 2. A crushed-limestone coarse aggregate was used with a maximum aggregate size of 19 mm along with natural sand and Type I portland cement. The FRC mixture incorporated a structural synthetic fiber at a dosage of 0.78% by volume, which is equivalent to 7.2 kg/m³ (12.1 lb/yd³). This fiber content was chosen because it would be the maximum feasible amount practically used by engineers in the field. Table 3 shows the properties of the synthetic fiber.

The plain and FRC batches were mixed at approximately the same time. The layered specimen shown in Figure 1 was created by first casting and consolidating the bottom layer (Material 2). The top layer (Material 1) was then placed into the mold. Consolidation of the top layer (Material 1) included 25-mm penetration into the bottom layer (Material 2) to ensure a graded interface zone between the two materials. The specimens were moist cured for 7 days before

TABLE 3 Properties of Synthetic Fibers

Fiber Type	Synthetic Fiber
Photo	
Material	Polypropylene–polyethylene
Cross section	Rectangular
Length (mm)	40
Thickness (mm)	0.105
Width (mm)	1.4
Aspect ratio	90
Specific gravity	0.92
Tensile capacity (MPa)	620
Modulus of elasticity (GPa)	9.5

testing. One day before testing, a notch one-third of the specimen depth was cut into each specimen.

The compressive and split tensile strengths of each mixture were determined without layering the materials in the cylinders (102 mm in diameter by 203 mm in length). The compressive strength and split tensile strengths at 7 days are shown in Table 2. The addition of fibers did not affect the compressive strength of the plain concrete, but the higher fiber content mixtures resulted in slightly increased split tensile strength over plain concrete, a result that is typically seen when fiber contents approach 1% (11, 15).

TEST RESULTS AND CALCULATION OF FRACTURE PARAMETERS

Use of TPFM

For numerical simulation of the fracture behavior of the functionally layered concrete specimens, the TPFM (12) was first used to quantify the fracture parameters of the monolithic concrete beam specimens (PCC or FRC). The TPFM idealizes the nonlinear fracture behavior of concrete materials by assuming an effective elastic crack and then employing linear elastic fracture mechanics. The notched TPB specimens in Figure 1 were used to derive two fracture parameters. The TPB dimensions were $700 \times 150 \times 80$ mm, and the initial notch depth (a_0) was 50 mm. The beam specimen had a ligament depth of $h - a_0$, and therefore

$$h_1 = h_2 - a_0 \quad (1)$$

This arrangement ensured that the effective cross-sectional area in one layer was equal to that in the other layer. In the TPB specimen with $h = 150$ mm and $a_0 = 50$ mm, the depth of Layer 1 was $h_1 = 50$ mm and $h_2 = 100$ mm.

The testing guidelines for the TPFM are specified by the International Union of Testing and Research Laboratories for Materials and

Structures (13). The load (P) and crack mouth opening displacement (CMOD) are recorded. Each TPB specimen was subjected to 10 cycles of loading and unloading that were followed by a final cycle of loading until the beam fractured or the CMOD gauge went out of range. Figure 2 shows the monotonic load–CMOD curve for a PCC specimen and also the envelope curve encompassing the load–unload cycles.

Two fracture parameters, critical stress intensity factor (K_{IC}) and crack tip opening displacement (CTOD_c), were calculated from the loading and unloading compliance curves. The loading and unloading compliance values were determined from the first load–unload cycle, as shown in Figure 2. The loading compliance (C_l) was calculated as the inverse of the slope from zero until the load reached half the peak load ($\frac{1}{2}P_c$). The specimen was unloaded after the load decreased 5% from the peak load. The unloading compliance (C_u) was calculated as the inverse of the slope of the unloading curve from 80% of the peak load of the cycle until the minimum load.

The K_{IC} and CTOD_c were calculated by first obtaining the critical effective crack length (a_c) at the peak load. This was completed by equating the modulus of elasticity obtained with the loading and unloading compliances, E_l and E_u , respectively:

$$E_l = \frac{6sa g_2(\alpha_0)}{C_l w^2 t} \quad (2)$$

$$E_u = \frac{6sa_c g_2(\alpha_c)}{C_u w^2 t} \quad (3)$$

where

s = span,

a_0 = initial notch depth of the beam,

$g_2(\alpha)$ = opening displacement geometric factor for the TPB specimen,

α_0 = initial notch–depth ratio for the TPB specimen,

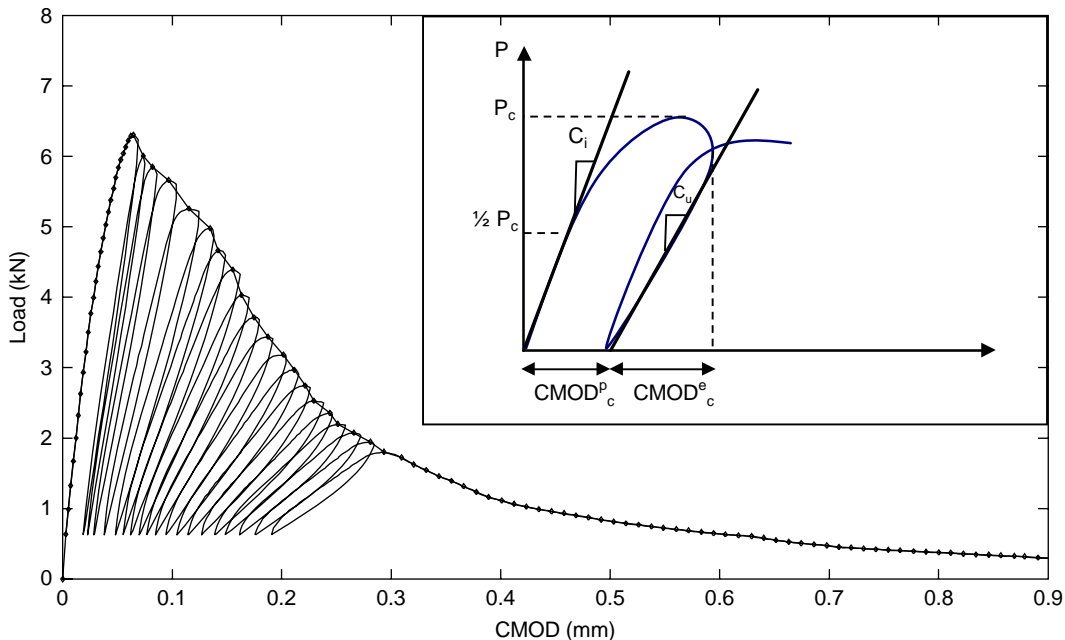


FIGURE 2 Load–CMOD curve for plain concrete specimen with compliance cycles and envelope curve and (inset) definition of loading and unloading compliance (C_l and C_u) from plot of load (P) versus CMOD.

α_c = critical notch–depth ratio for the TPB specimen,
 w = depth, and
 t = width.

Once a_c is computed, then the critical stress intensity factor (K_{IC}) can be calculated from Equation 4:

$$K_{IC} = 3(P_c + 0.5W_0 s/l) \frac{s\sqrt{\pi a_c} g_1(a_c/w)}{2w^2 t} \quad (4)$$

where

P_c = peak load,
 W_0 = self-weight of the specimen,
 l = length of the specimen, and
 g_1 = geometric function for the beam specimen defined as

$$g_1\left(\frac{a_c}{w}\right) = \frac{1.99 - (a_c/w)(1 - a_c/w) \left[\begin{array}{l} 2.15 - 3.93(a_c/w) \\ + 2.70(a_c/w)^2 \end{array} \right]}{\sqrt{\pi} [1 + 2(a_c/w)][1 - (a_c/w)]^{3/2}} \quad (5)$$

Finally, the CTOD_c is calculated with Equation 6:

$$CTOD_c = 6(P_c + 0.5W_0 s/l) * \frac{sa_c g_2(a_c/w)}{Ew^2 t} * \left[\begin{array}{l} (1 - (a_c/a_0))^2 + \left[1.081 - 1.149 \left(\frac{a_c}{w} \right) \right] \\ * \left[(a_c/a_0) - (a_c/a_0)^2 \right] \end{array} \right]^{1/2} \quad (6)$$

with $g_2(\alpha)$ given by

$$g_2(\alpha) = 0.76 - 2.28\alpha + 3.87\alpha^2 - 2.04\alpha^3 + \frac{0.66}{(1 - \alpha)^2} \quad (7)$$

For plane stress, the energy release rate G_f (or initial fracture energy) is related to K_{IC} and the modulus of elasticity, E , by the following equation:

$$G_f = \frac{K_{IC}^2}{E} \quad (8)$$

Table 4 presents the average P_c , K_{IC} , G_f , a_c , and CTOD_c results from TPB tests. The use of fibers did not significantly affect the peak load of the specimens and subsequently did not significantly change the calculated K_{IC} , G_f , or CTOD_c. Furthermore, the critical crack length is similar from one sample to the next. These properties are related only to the stage of crack initiation and not to crack propagation; the initial properties did not differ much because the same

concrete constituents and proportions were used for both the PCC and FRC specimens.

Total Fracture Energy

The total fracture energy (G_F), calculated on the basis of a method proposed by Hillerborg (14), is defined as the ratio between the total energy (W_t) and the concrete fracture area $(w - a_0)t$. W_t is calculated by using the sum of the area under the curve for the raw load (P_a) versus the CMOD envelope (W_r) and $P_w \delta_0$, where P_a is the raw load applied by the testing machine (without considering self-weight), P_w is the equivalent self-weight force, and δ_0 is the CMOD displacement corresponding to $P_a = P_0$ at failure, where P_0 is the seating load at 0.05 kN. The raw load versus CMOD for each layered system is shown in Figure 3. The equivalent self-weight force is calculated as $P_w = (s/2l)W_0$, where the variables are defined as noted earlier.

The total fracture energy was calculated as

$$G_F = \frac{W_t}{(w - a_0)t} = \frac{W_r + 2P_w \delta_0}{(w - a_0)t} \quad (9)$$

Due to fibers' ability to bridge cracks effectively, the load can remain constant until large values of CMOD, as Figure 4 shows. To determine the total fracture energy of the FRC beams and not the fracture energy at any arbitrary opening displacement, additional TPB tests were performed with a linear variable displacement transformer to measure the CMOD until the raw load reached approximately zero, as Figure 4 also shows. The area under the envelope curve until failure ($P_a = P_0$) and a CMOD_{max} = $\delta_0 = 2$ mm were then used to calculate two fracture energy quantities for the FRC, respectively: total fracture energy (G_F) and relative fracture energy (G_{2mm}). The relative fracture energy calculated at a 2-mm opening displacement was selected because many CMOD devices have ranges from 2 to 4 mm and the maximum crack width desired in fractured concrete slabs is typically between 1 and 2.5 mm.

Figure 3 does not show a significant difference in peak loads between specimens, with all peaks in the range of 3.48 and 3.71, which is a coefficient of variation of just 6%. However, big differences are apparent when the areas under the different load–CMOD curves are compared. As Figure 3 shows, the FRC-FRC and PCC-FRC specimens had significantly better fracture resistance than the PCC-PCC specimens. The FRC-PCC specimens still behaved better than PCC but had a lower residual strength than the other FRC specimens. Table 4 shows that fibers dispersed throughout the full depth of the beam increased the G_{2mm} by 218% over PCC. Specimens with PCC on top and FRC on the bottom (PCC-FRC) had a higher G_{2mm} than samples with FRC on top and PCC on the bottom (FRC-PCC). The addition of fibers to the bottom and the top layer improved G_{2mm} by 108% and 80%, respectively, in comparison with PCC-PCC.

TABLE 4 Average Fracture Parameters for TPB Specimens

Top and Bottom Layers	P_c (kN)	K_{IC} (MPa • m ^{1/2})	CTOD _c (mm)	G_f (N/m)	a_c (mm)	G_{2mm} (N/m)	G_F (N/m)
PCC-PCC	3.710	1.01	0.016	38.3	61.8	120	120
FRC-FRC	3.482	1.03	0.016	37.1	66.5	381	3,531
PCC-FRC	3.714	1.08	0.017	40.5	65.7	249	—
FRC-PCC	3.569	0.97	0.016	35.4	61.6	216	—

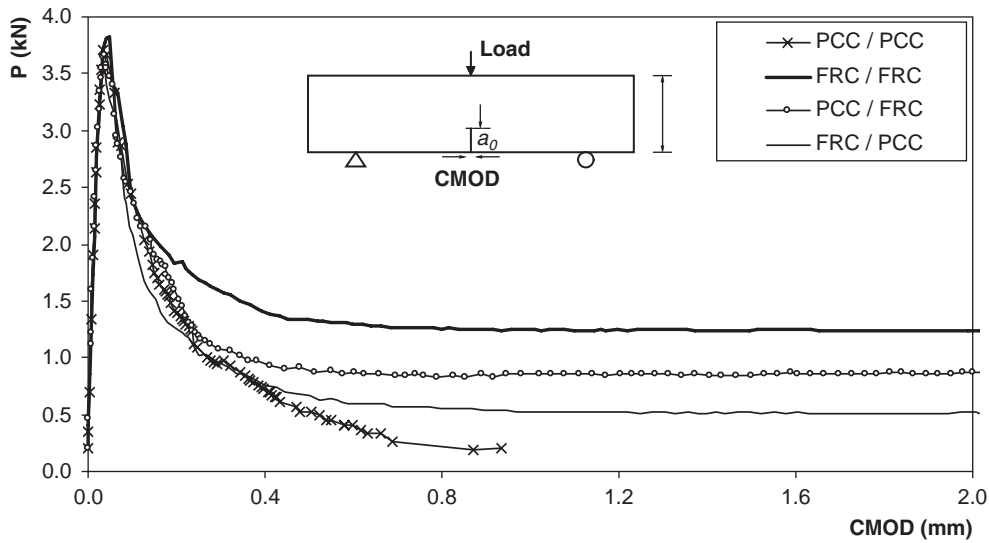


FIGURE 3 Average load-CMOD envelope curves for TPB specimens with plain, synthetic fiber, and functionally layered concrete.

NUMERICAL MODELING FOR NONLINEAR FRACTURE PROCESS ZONE

General Description

For numerical prediction of the fracture behavior of the FGCM shown in Figure 3, a finite element-based model that can describe the nonlinear fracture process zone in concrete materials is required. This objective is achieved by first defining a mesh with bulk elements that represent the material at the top and the bottom layers, as shown in Figure 5a. This mesh is refined close to the crack tip, and cohesive elements are inserted in the expected crack path. These cohesive elements, shown in Figure 5b, require a softening model to represent the fracture behavior of the material in the respective layers (i.e., plain concrete and FRC). This numerical model must be able to predict the constitutive behavior of PCC-PCC and FRC-FRC specimens as well as the FGCM samples, PCC-FRC and FRC-PCC.

Softening Model for Plain Concrete

Under monotonically increasing load, progressive cracking in plain concrete can be idealized as a zone of distributed microcracks, a bridging zone, and a traction-free macrocrack zone, as shown in Figure 6a. Microcracks initiate ahead of the bridging zone before the applied stress reaches the material's tensile strength (f'_t). When the stress reaches the tensile strength, microcracks grow and coalesce, a process that produces the bridging zone, also called the nonlinear fracture process zone. This zone results from the crack branching and interlocking as a result of the weak interface between the aggregates and cement matrix (16, 17). The nonlinear process zone connects the microcrack and a traction free macrocrack zone. When a crack opening width is greater than a certain value, called the final crack opening width (w_f), a macroscopic crack that cannot transfer traction along its surfaces anymore appears.

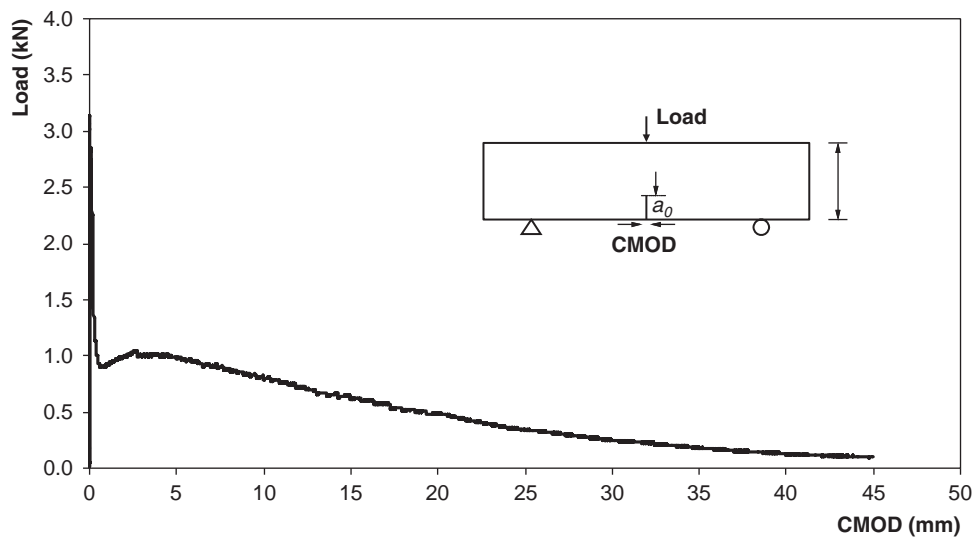


FIGURE 4 Average load-CMOD envelope curve for TPB specimen with FRC.

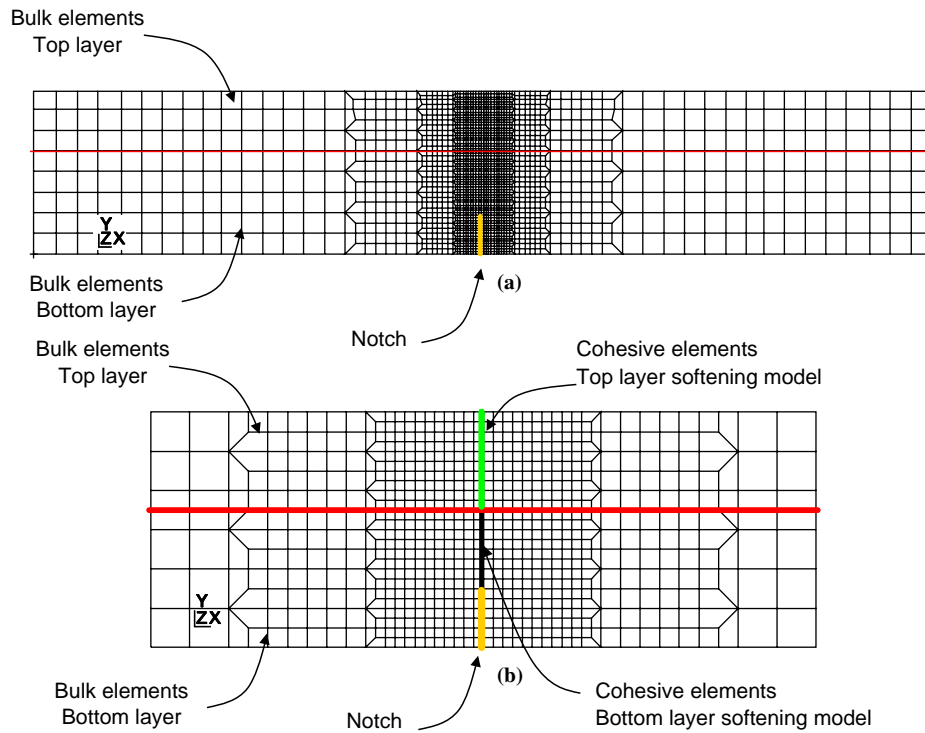


FIGURE 5 Representations of (a) finite element mesh and (b) detail of mesh along cohesive element region.

The nonlinear fracture process zone for concrete is best characterized by the cohesive zone model (CZM) (18), as shown in Figure 6a. The softening curve in the CZM is physically defined by four experimental fracture parameters (19): tensile strength, initial fracture energy (G_f), total fracture energy (G_F), and critical crack tip opening displacement (CTOD). The initial fracture energy defines the horizontal axis intercept (w_1) of the initial softening slope (20), expressed as

$$w_1 = \frac{2G_f}{f'_t} \quad (10)$$

The kink point of the crack opening width (w_k) is hypothesized (19) as

$$w_k = \text{CTOD}_c \quad (11)$$

which results in the determination of the stress ratio (Ψ) at the kink point:

$$\Psi = 1 - \frac{\text{CTOD}_c f'_t}{2G_f} \quad (12)$$

The final crack opening width is calculated as

$$w_f = \frac{2}{\Psi f'_t} [G_F - (1 - \Psi)G_f] \quad (13)$$

which is obtained by equating the total fracture energy with the area under the softening model for PCC (14).

Softening Model for FRC

Fracture mechanisms of FRC are different from those of PCC due to the effect fibers have on the nonlinear fracture process zone (17), as shown in Figure 6b. Although fibers do not generally influence the tensile strength or early postpeak behavior at low-volume fractions, fibers increase the total fracture energy of PCC, which results in the observed high postpeak load behaviors (15). These same features can be observed in the softening curves shown in Figures 3 and 4. As a result, the nonlinear fracture process zone for FRC is further divided into the aggregate bridging zone and the fiber bridging zone, as shown in the model diagrammed in Figure 6b. The aggregate bridging zone is represented by the same softening model for PCC. The fiber bridging zone is characterized by a linear descending slope (21), which itself characterizes the fiber debonding and pullout mechanisms.

The softening model for FRC is determined by the total fracture energy (G_{FRC}) and w_f of FRC and four experimental fracture parameters (f'_t , G_f , G_F , CTOD_c) of PCC. G_{FRC} is the fracture energy from the full load-CMOD curve, as shown in Figure 4. Because fibers have limited influence on the aggregate bridging zone, the first kink point (w_{k1} , $\Psi_1 f'_t$) in the softening model for FRC is the same as the kink point (w_k , $\Psi f'_t$) in the model for PCC. The second kink point (w_{k2} , $\Psi_2 f'_t$) is evaluated with the total fracture energy of FRC (G_{FRC}) and the assumption of w_f , expressed as

$$\Psi_2 = \frac{2(G_{\text{FRC}} - G_f)}{f'_t(w_f - w_2)} \quad (14)$$

and

$$w_{k2} = w_2 - \frac{\Psi_2}{\Psi_1} (w_1 - w_{k1}) \quad (15)$$

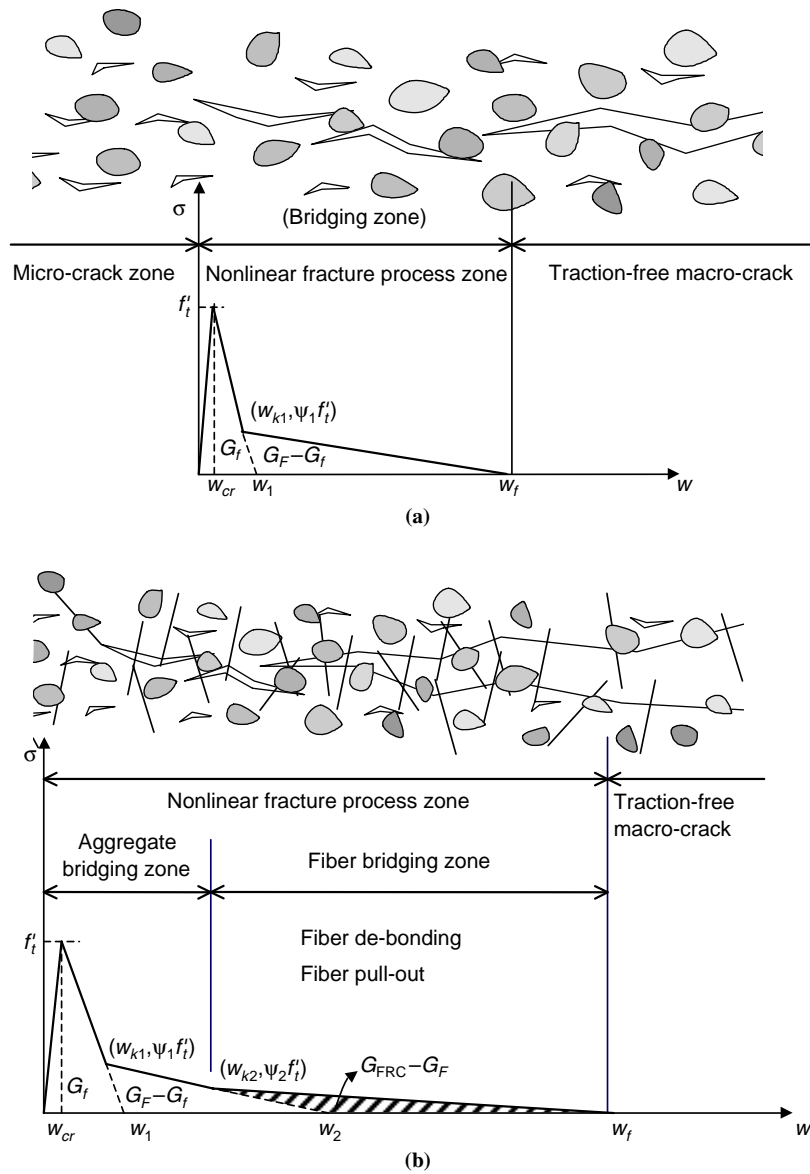


FIGURE 6 Fracture mechanisms and experimental fracture parameter-based softening model for (a) plain concrete and (b) fiber-reinforced concrete.

In this study, the final crack opening width was estimated as a quarter or half the fiber length ($L/4$ or $L/2$), which corresponds to the averaged pullout length for randomly distributed fibers reported in the literature (22–24). Ongoing research is being conducted to provide a basis for the w_f estimation, given a specific fiber type and concrete matrix.

Comparison Between Experimental and Numerical Results

The bulk finite element model (FEM) with the CZMs proposed for PCC and FRC were implemented into the commercial finite element program Abaqus as a user element subroutine. On the basis of previous convergence studies (25), the size of the cohesive element was selected to be 1 mm. Figure 7 illustrates the correspondence between

the experimental fracture results and the numerical simulations for the different combinations of concrete layers. The CZMs based on the measured fracture parameters of the PCC and FRC were successfully able to represent the fracture behavior of not only PCC and FRC specimens but also FGCM specimens (FRC-PCC and PCC-FRC). As Figure 7 shows, the FEM with $w_f = L/4$ demonstrated the upper bound of the fracture behavior of the FRC-FRC and PCC-FRC beams, while the model with $w_f = L/2$ illustrated the lower bound of the experimental fracture behavior.

Other numerical simulation models were compared by using the FRC-FRC test data, as Figure 8 shows. A bilinear cohesive zone softening model used for the plain concrete mixtures was implemented on the basis of total fracture energy (G_{FRC}). The bilinear softening model did not accurately represent the postpeak behavior of the FRC beam. Final crack opening widths (w_f) of $L/2$ and $L/4$ (half and quarter the fiber length, respectively) were simulated by using

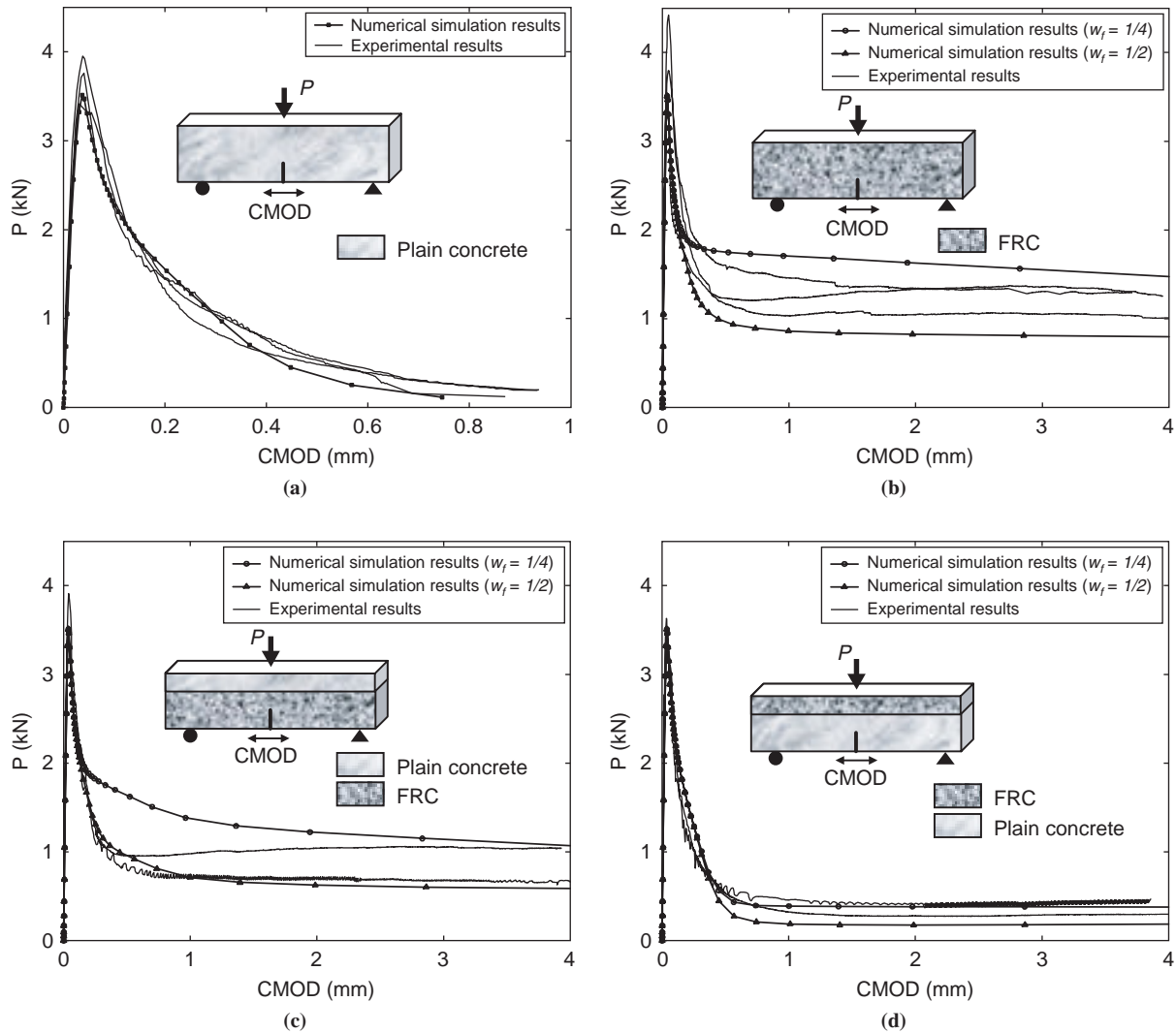


FIGURE 7 Comparison between experimental and numerical simulation results for (a) plain concrete (PCC-PCC), (b) fiber-reinforced concrete (FRC-FRC), (c) FRC layer at the bottom (PCC-FRC), and (d) FRC layer at the top (FRC-PCC).

the trilinear softening model. Numerical simulation of $L/2$ underestimated the postpeak curve but was similar to the experimental data of the FRC beam at low CMOD values. When $w_f = L/4$ was used in the numerical simulation, the postpeak response was overestimated but showed a reasonable match to the experimental data at higher CMOD values. Figure 9 demonstrates that the FGCM fracture behavior can be predicted, as is the case in which the FRC layer at the notch location (PCC-FRC) results in a higher postpeak response than when the FRC layer is cast in the top part of the specimen (FRC-PCC).

EFFECT OF LAYERING ON SPECIMEN FRACTURE BEHAVIOR

When synthetic fibers were used, the specimens with FRC on the bottom had higher fracture energy (G_{2mm}) relative to the specimen with FRC on the top. This result occurred because the synthetic-fibers modulus is closer to the concrete matrix modulus and allows for effective crack bridging behind the crack front. Because of the

lower amount of fiber bridging behind the crack front, synthetic fibers near the top of the specimen were not able to dissipate as much energy.

This preliminary testing suggests that the use of FGCM for rigid pavement can optimize the materials and concrete pavement fracture behavior. The accompanying numerical analysis based on the CZM formulation was also able to predict reasonably the fracture behavior of the FGCM. This numerical analysis tool is essential to quantifying of the fracture behavior of various concrete materials, thicknesses, and placements within the surface concrete layer for future FGCM systems (26), because excessive testing would be required to quantify the fracture behavior of all fiber types, volume fractions, layer depths, and concrete mixture designs.

The proof of concept testing and analysis presented has shown that concrete material properties and placement in a structure can affect the fracture behavior of the system. Improvements in the overall fracture behavior of concrete pavements can be realized and result in thinner slabs and fewer joints. Furthermore, FGCM enables use of lower-quality construction materials, such as recycled concrete, in certain regions of the slab without sacrificing overall pavement performance.

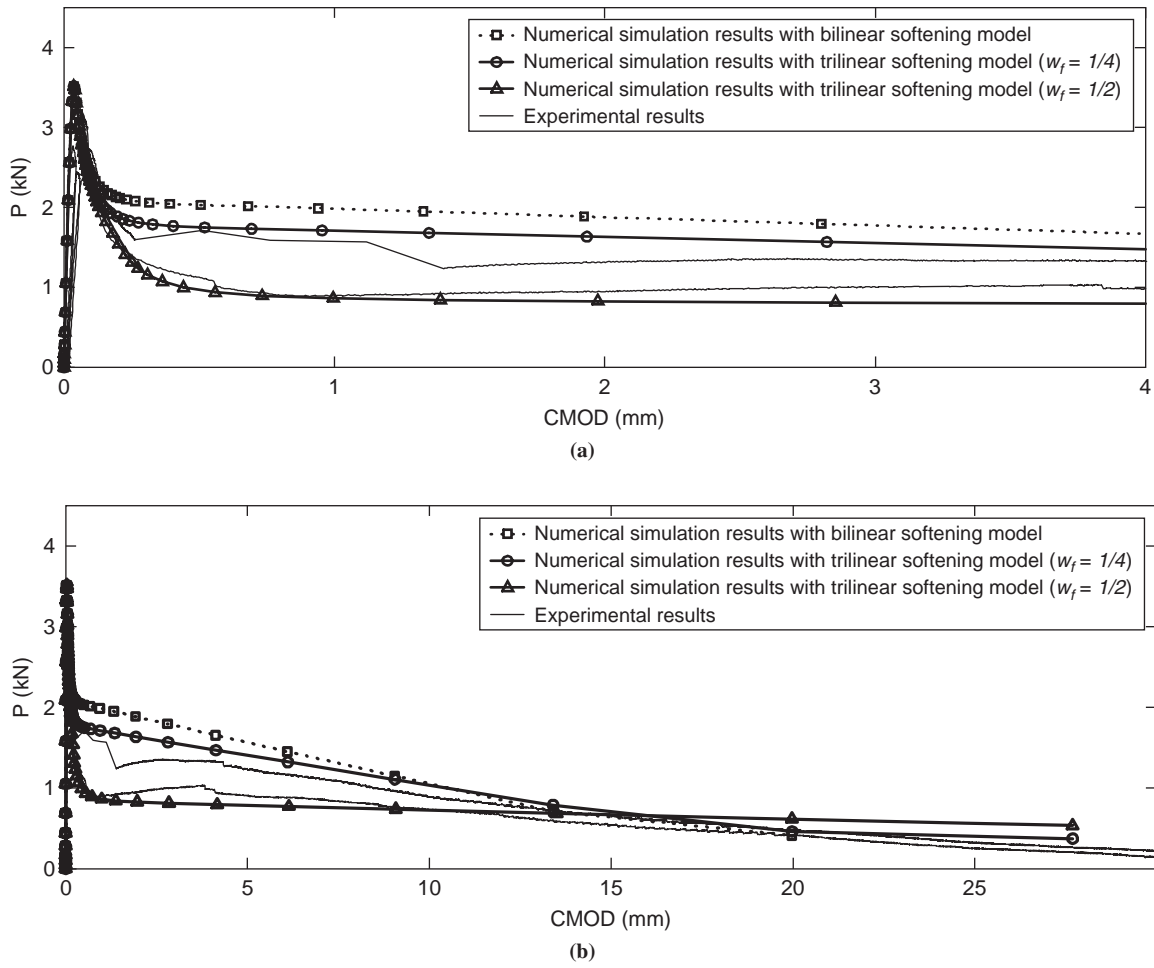


FIGURE 8 Comparison between experimental results and numerical simulation of FRC specimens (a) for the first 4-mm opening displacement and (b) until final specimen failure.

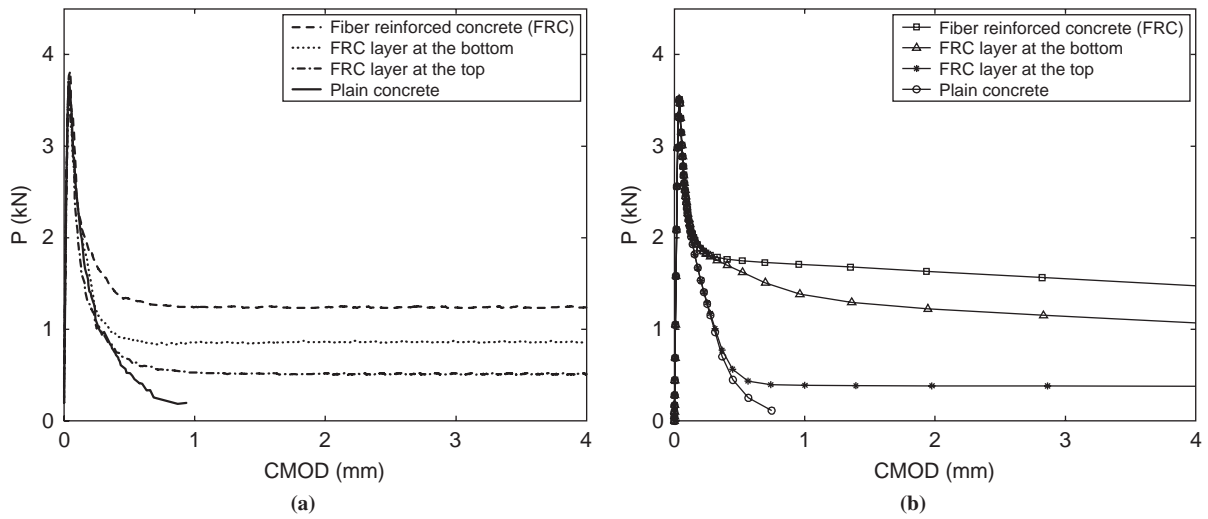


FIGURE 9 Comparison between (a) experimental results and (b) numerical simulation of TPB specimens ($w_f = L/4$).

CONCLUSION

The application of FGCM (or functionally layered concrete materials) for rigid pavement has shown promising results in fracture testing and numerical modeling. As expected, all concrete specimens that used fibers showed an improved residual strength or softening behavior over PCC. The initial fracture energy and critical crack tip opening displacement did not distinguish the differences in fracture behavior of the PCC, FRC, and functionally layered concrete. The total fracture energy (G_F) or the fracture energy up to 2-mm opening displacement (G_{2mm}) was the key indicator in quantifying how the FRC and FGC improved the cracking resistance of PCC specimens. The improvement in the concrete G_{2mm} was closely related to the depth and position of the fibrous concrete layer. The FGCM with FRC was more fracture resistant (increased G_{2mm}) when the fibers were placed closest to the notch and slightly less efficient when the fibers were placed near the top of the specimen. The fiber bridging mechanism behind the crack front was the primary mechanism that resulted in a higher residual load capacity.

An integrated approach that involved testing and modeling was successfully implemented in this research investigation. A finite element-based CZM was developed to predict the softening behavior of the FGCM systems on the basis of the individual concrete material fracture properties. The numerical simulation of FGCM, based on the measured PCC and FRC fracture parameters, was able to match the experimental results of the various combinations of PCC and FRC. The CZM prediction of the experimental results was promising and demonstrated the viability of FGCM and the CZM for characterizing and designing layered concrete pavement systems.

ACKNOWLEDGMENTS

The authors acknowledge support through the Center of Excellence for Airport Technology provided by the O'Hare Modernization Program and the City of Chicago for their financial support in this study.

REFERENCES

- Hirano, T., J. Teraki, and T. Yamada. On the Design of Functionally Graded Materials. *Proc., 1st International Symposium on Functionally Graded Materials* (M. Ymanouchi, M. Koizumi, T. Hirai, and L. Shiota, eds.), Sendai, Japan, 1990, pp. 5–10.
- Hirai, T. Functionally Graded Materials and Nanocomposites. *Proc., 2nd International Symposium on Functionally Graded Materials* (J. B. Holt, M. Koizumi, T. Hirai, and Z. A. Munir, eds.), in *Ceramic Transactions*, Vol. 34, 1993, pp. 11–20.
- Miyamoto, Y., W. A. Kaysser, B. H. Rabin, A. Kawasaki, and R. G. Ford. *Functionally Graded Materials: Design, Processing and Applications*. Kluwer Academic Publishers, Dordrecht, Netherlands, 1999.
- Paulino, G. H., Z.-H. Jin, and R. H. Dodds. Failure of Functionally Graded Materials. In *Comprehensive Structural Integrity, Volume 2: Fundamental Theories and Mechanisms of Failure* (B. L. Karihaloo and W. G. Knauss, eds.). Elsevier, Amsterdam, Netherlands, 2003, pp. 607–644.
- Ilschner, B. Technical Resume of the 5th International Symposium on Functionally Graded Materials. *Materials Science Forum*, Vols. 308–311, 1999, pp. 3–10.
- Darter, M. I. *Report on the 1992 U.S. Tour of European Concrete Highways*. FHWA, U.S. Department of Transportation, 1992, 124 pp.
- Smiley, D. L. *First-Year Performance of the European Concrete Pavement on Northbound I-75—Detroit, Michigan*. Michigan Department of Transportation, Lansing, 1995, 22 pp.
- Cable, J. K., and D. P. Frentress. *Two-Lift Portland Cement Concrete Pavements to Meet Public Needs*. FHWA, U.S. Department of Transportation, 2004.
- Ravindrarajah, R. S., and C. T. Tam. Flexural Strength of Steel Fibre Reinforced Concrete Beams. *International Journal of Cement Composites and Lightweight Concrete*, Vol. 6, No. 4, 1984, pp. 273–278.
- Zhang, J., and V. C. Li. Monotonic and Fatigue Performance in Bending of Fiber-Reinforced Engineered Cementitious Composite in Overlay System. *Cement and Concrete Research*, Vol. 32, 2002, pp. 415–423.
- Balaguru, P., and S. P. Shah. *Fiber-Reinforced Cement Composites*. McGraw-Hill, New York, 1992.
- Jenq, Y., and S. P. Shah. Two Parameter Model for Concrete. *Journal of Engineering Mechanics*, Vol. 111, No. 10, 1985, pp. 1227–1241.
- RILEM Committee on Fracture Mechanics of Concrete-Test Methods. Determination of the Fracture Parameters (K_{IC} and CTOD_c) of Plain Concrete Using Three-Point Bend Tests. *Materials and Structures*, Vol. 23, 1990, pp. 457–760.
- Hillerborg, A. The Theoretical Basis of a Method to Determine the Fracture Energy GF of Concrete. *Material and Structures*, Vol. 16, 1985, pp. 291–296.
- Shah, S. P. Do Fibers Increase the Tensile Strength of Cement-Based Matrixes? *Materials Journal*, Vol. 88, No. 6, 1991, pp. 595–602.
- Anderson, T. L. *Fracture Mechanics: Fundamentals and Applications*. CRC Press, Boca Raton, Fla., 1995.
- Van Mier, J. G. M. *Fracture Processes of Concrete: Assessment of Material Parameters for Fracture Models*. CRC Press, Boca Raton, Fla., 1996.
- Roesler, J. R., G. H. Paulino, K. Park, and C. Gaedicke. Concrete Fracture Prediction Using Bilinear Softening. *Cement and Concrete Composites*, Vol. 29, 2007, pp. 300–312.
- Park, K. *Concrete Fracture Mechanics and Size Effect Using a Specialized Cohesive Zone Model*. MS thesis. University of Illinois at Urbana-Champaign, 2005.
- Bazant, Z. P., and M. T. Kazemi. Determination of Fracture Energy, Process Zone Length and Brittleness Number from Size Effect, with Application to Rock and Concrete. *International Journal of Fracture*, Vol. 44, 1990, pp. 111–131.
- Roesler, J. R., A. Bordelon, C. Gaedicke, K. Park, and G. H. Paulino. Fracture Behavior of Properties of Functionally Graded Fiber-Reinforced Concrete. *Proc., Multiscale and Functionally Graded Materials Conference*, Ko Olina, Hawaii, American Institute of Physics, Melville, N.Y., 2006.
- Gopalaratnam, V. S., and S. P. Shah. Tensile Failure of Steel Fiber-Reinforced Mortar. *Journal of Engineering Mechanics*, Vol. 113, No. 5, 1987, pp. 635–652.
- Fu, S. Y., and B. Lauke. Effects of Fiber Length and Fiber Orientation Distributions on the Tensile Strength of Short-Fiber-Reinforced Polymers. *Composites Science and Technology*, Vol. 56, No. 10, 1996, pp. 1179–1190.
- Lok, T. S., and J. S. Pei. Flexural Behavior of Steel Fiber Reinforced Concrete. *Journal of Materials in Civil Engineering*, Vol. 10, No. 2, 1998, pp. 86–97.
- Song, S. H., G. H. Paulino, and W. G. Buttlar. Simulation of Crack Propagation in Asphalt Concrete Using a Cohesive Zone Model. *Journal of Engineering Mechanics*. Vol. 132, No. 11, 2006, pp. 1215–1223.
- Altoubat, S. A., J. R. Roesler, D. A. Lange, and K.-A. Rieder. Simplified Method for Concrete Pavement Design with Discrete Structural Fibers. *Construction and Building Materials*, 2007 (forthcoming).

The information presented in this paper is the responsibility of the authors and does not reflect the views of the sponsoring agencies.

The Rigid Pavement Design Committee sponsored publication of this paper.